LETTER • OPEN ACCESS

The role of eddy-wind interaction in the eddy kinetic energy budget of the Agulhas retroflection region

To cite this article: Yanan Zhu *et al* 2023 *Environ. Res. Lett.* **18** 104032

View the article online for updates and enhancements.

ENVIRONMENTAL RESEARCH
LETTERS

LETTER

The role of eddy-wind interaction in the eddy kinetic energy budget of the Agulhas retroflection region

Yanan Zhu[1],* , Yuanlong Li[1,2], Yang Yang[3] and Fan Wang[1,2],*

[1] CAS Key Laboratory of Ocean Circulation and Waves, Institute of Oceanology, Qingdao, People's Republic of China
[2] Laoshan Laboratory, Qingdao, People's Republic of China
[3] State Key Laboratory of Marine Environmental Science, College of Ocean and Earth Sciences, Xiamen University, Xiamen, People's Republic of China
* Authors to whom any correspondence should be addressed.

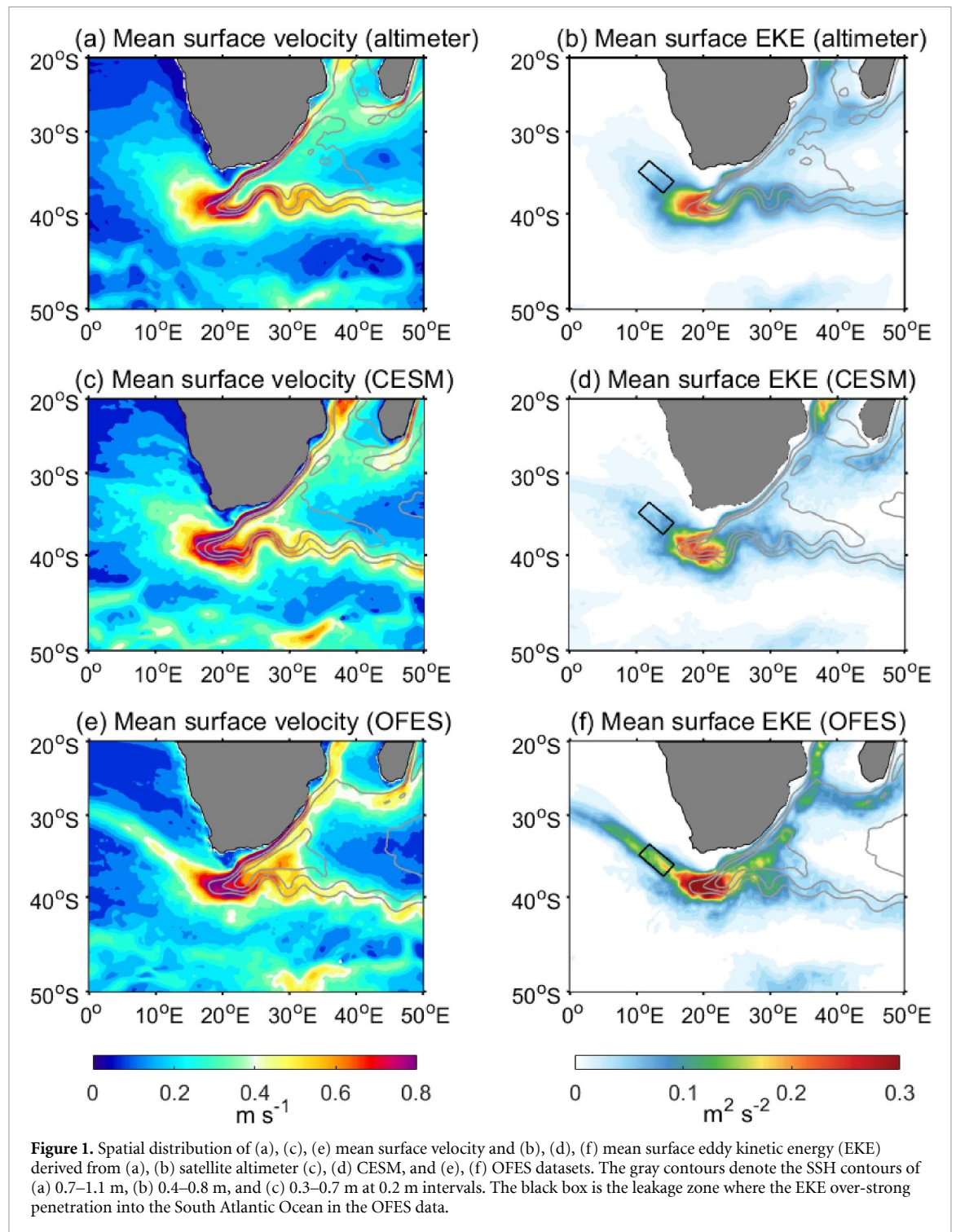E-mail: yzhu@qdio.ac.cn and fwang@qdio.ac.cn

Abstract

The Agulhas retroflection (AR) region possesses the highest eddy kinetic energy (EKE) level in the Indian Ocean. However, mechanisms regulating EKE of the AR remain uncertain. Here, by analyzing an eddy-resolving coupled model simulation with improved EKE representation, we show that the upper-ocean EKE of the AR is mainly generated through barotropic instability in its upstream and leakage zones and is by nonlocal transport in its downstream zone. The interaction between mesoscale eddies and local winds plays a key role in EKE dissipation. The lack of eddy-wind interaction results in flawed EKE budget in the leakage zone in ocean-alone models, leading to severe biases in EKE distribution with overestimation and over-strong penetration into the South Atlantic. Our results highlight the essence of mesoscale air-sea interaction in the dynamics of the AR, with implications for understanding the inter-basin transport of the Agulhas leakage.

1. Introduction

The Agulhas Current (AC) is the poleward-flowing western boundary current of the subtropical Southern Indian Ocean with a mean transport of 77 Sv (1 Sv = 10^6 m^3 s^{-1}; Beal *et al* 2015). Upon reaching the southern tip of the African continent, it separates from the coast and retroflects east to feed the Agulhas return current (ARC) (Lutjeharms and Ansorge 2001), forming the Agulhas retroflection (AR) point (Lutjeharms and Van Ballegooyen 1988). The AR regime possesses the highest eddy kinetic energy (EKE) in the Indian Ocean (Zhu *et al* 2018). Rings and eddies generated from the AR serve as conveyors for the warm and salty Indian Ocean water to the Southern Atlantic Ocean, constituting the inter-basin transport of the Agulhas leakage (Gordon 1985, Biastoch *et al* 2008). As a key feature of the AC system (Beal *et al* 2011), the AR is subjected to dynamic complexities and is worthy of in-depth investigation.

Mesoscale eddy activity (quantified by surface EKE) is crucial for the AR dynamics; it regulates zonal displacements of the AR point (Zhu *et al* 2021) and the formation of Agulhas leakage (Beal *et al* 2011). Eddy-resolving ocean model simulations are widely utilized in understanding the EKE budget of the AC system (Zhu *et al* 2018, Adeagbo *et al* 2022, Li *et al* 2023). Meanwhile, these studies also reveal common biases (although model-dependent in quantity) in these models, typically with over-strong penetration of EKE toward the South Atlantic (Maltrud and McClean 2005, Thoppil *et al* 2011, Renault *et al* 2017). These biases hinder the understanding of AR dynamics and lead to substantial uncertainties in the simulated Agulhas leakage in these ocean-alone models, with the transport ranging widely from 2 to 18 Sv (Biastoch *et al* 2008).

Existing studies suggest that the simulations of leakage transport and pathways of Agulhas rings are generally more realistic in coupled climate models,

Figure 1. Spatial distribution of (a), (c), (e) mean surface velocity and (b), (d), (f) mean surface eddy kinetic energy (EKE) derived from (a), (b) satellite altimeter (c), (d) CESM, and (e), (f) OFES datasets. The gray contours denote the SSH contours of (a) 0.7–1.1 m, (b) 0.4–0.8 m, and (c) 0.3–0.7 m at 0.2 m intervals. The black box is the leakage zone where the EKE over-strong penetration into the South Atlantic Ocean in the OFES data.

with mesoscale air-sea interaction is taken into consideration (Putrasahan *et al* 2015, Chen *et al* 2016). Notably, the interaction between eddies and winds represents a major contributor to EKE dissipation (10%–50%) in eddy-rich regions (Eden and Dietze 2009, Gaube *et al* 2015, Seo *et al* 2016) such as the AC system (Renault *et al* 2017). This damping effect is through eddy-induced wind stress anomalies (Renault *et al* 2016) and Ekman pumping (Gaube *et al* 2015). Moreover, neglecting the eddy-wind interaction may lead to an overestimation of the total wind

work on the ocean and affect the simulated mean circulation (Pacanowski 1987, Luo *et al* 2005, Duhaut and Straub 2006, Scott and Xu 2009).

In this study, we aim to investigate the EKE budget in the upstream, downstream, and leakage zones of the AR by contrasting simulations of a coupled model and an ocean-alone model with similar resolutions. We show that the EKE distribution in the AR region is more realistically simulated by the coupled model, as referenced to satellite observations (figure 1). Further analysis confirms that mesoscale air-sea interaction

play a crucial role in regulating EKE of the AR region and explains biases in ocean-alone models.

2. Data and method

2.1. Datasets

Here we analyze the high-resolution simulation of the Community Earth System Model (CESM) version 1.2.2 (Small *et al* 2014, Chu *et al* 2020, Huang *et al* 2021). The ocean model component of CESM is the Parallel Ocean Program version 2 (POP2) (Smith *et al* 2010), with horizontal resolutions of $0.1° \times 0.1°$ and 62 vertical levels and fully coupled to the $0.25°$ atmospheric model (Community Atmospheric Model 5) (Neale *et al* 2012), the Community Ice Code version 4 (Hunke and Lipscomb 2008), and Community Land Model version 4 (Lawrence *et al* 2011). The simulations are conducted for about 140 years with a 14 year spinup run (Small *et al* 2014). In this study, we use the daily results of the last six model year simulations to analyze the EKE budget in the AR region due to the big data size of three-dimensional CESM data. In addition, the EKE in the AR region is concentrated in the upper 500 m, especially in the upper 200 m (figure S1(b)).

In addition to the CESM model, we also use the output of the eddy-resolving ocean general circulation model (OGCM) for the Earth Simulator (OFES) (Masumoto *et al* 2004, Sasaki *et al* 2008) in this study. The OFES data is based on the Modular Ocean Model, version 3 (MOM3; Pacanowski and Griffies 2000), which is a 3D, z-level, hydrostatic, Boussinesq ocean model. It has a horizontal resolution of $0.1°$ and 54 vertical levels. Except for the different background viscosity and diffusivity coefficients of POP2 and MOM3 models, both of them use the KPP turbulent mixing closure scheme for mixing and bi-harmonic horizontal diffusion for vertical mixing in z-coordinate. There are three OFES simulations available (Climatological, NCEP-run, and QSCAT-run). The QSCAT-run simulation is used here due to the QSCAT wind is the highly spatiotemporal resolution observed wind that can resolve the mesoscale signals of wind. The QSCAT-run simulation is forced by the QSCAT winds from 20 July 1999 to 30 October 2009. As the AC has early retroflection in 2000–2001 (Dencausse *et al* 2010), the three day output of QSCAT-run OFES simulation from 2002 to 2007 (6 years like CESM data) is used in this study. It is note that the numbers of layers in the upper 500 m are similar in the OFES and CESM data, which are 29 and 32, respectively (figure S1(a)).

Daily satellite observational sea surface height and surface geostrophic velocity data used is the SSALTO/Data Unification and Altimeter Combination System (DUACS) multi-mission altimeter sea level product released in 2018 (DUACS-DT2018) with spatial resolution of $0.25°$ for the 1993–2019 period (Le Traon *et al* 1998, Taburet *et al* 2019).

2.2. Multiscale energy and vorticity analysis (MS-EVA) method

In this study, the EKE budget in the AR region is analyzed based on the MS-EVA method, which has been widely used in the energetic analysis in the Kuroshio extension (Yang and San Liang 2016) and the Gulf of Mexico (Yang *et al* 2020). For details of the MS-EVA method, see Liang and Robinson (2005) and Liang (2016). MS-EVA is based on a new functional analysis tool, namely, the multiscale window transform (MWT), which is developed for a physically faithful representation of multiscale energy (Liang and Anderson 2007). With the MWT, the original fields can be decomposed into several orthogonal scale windows (Liang 2016). Here, we decompose the variables into three windows:

$$A = A^{\sim 0} + A^{\sim 1} + A^{\sim 2}, \tag{1}$$

where $A^{\sim 0}$, $A^{\sim 1}$, and $A^{\sim 2}$ represents the reconstructions of mean flow, mesoscale eddies, and high-frequency processes, respectively. The high-frequency processes include submesoscale eddies, oceanic turbulence, and other unresolved subgrid processes (Yang and San Liang 2016).

The oceanic mesoscale eddy signals are associated with temporal scales of 30–270 d in the AC system (Zhu *et al* 2018, 2021). In this study, the cutoff period is set to 260 d between the mean flow and mesoscale eddies, and 30 d between mesoscale eddies and high-frequency processes, respectively. Note that changing the cutoff periods from 240 d (20 d) to 300 d (50 d) has no significant impact in the results. Within the MWT framework, the kinetic energy in the mesoscale eddy window is

$$\text{EKE} = \frac{1}{2}\rho_0 \widehat{\mathbf{u}}_H^{\sim 1} \cdot \widehat{\mathbf{u}}_H^{\sim 1} \tag{2}$$

where ρ_0 is the reference density, $\mathbf{u}_H = (u, v)$ is the horizontal velocity vector and the hat denotes the MWT operator. The detailed derivation of the kinetic energy equation is referred to Liang (2016). Here, the EKE budget equation is summarized in the following:

$$
\begin{aligned}
\frac{\partial}{\partial t}\text{EKE} = &- \left[\underbrace{\frac{1}{2}\rho_0\left(\hat{u}^{\sim 1}\right)^2 \nabla \cdot \hat{\mathbf{u}}_u^1 + \frac{1}{2}\rho_0\left(\hat{v}^{\sim 1}\right)^2 \nabla \cdot \hat{\mathbf{u}}_v^1}_{\Gamma_K^1} \right] \\
&- \underbrace{g\hat{\rho}^{\sim 1}\hat{w}^{\sim 1}}_{b^1} \\
&- \nabla \cdot \left[\underbrace{\frac{1}{2}\rho_0\hat{\mathbf{u}}^{\sim 1}(\widehat{\mathbf{u}\mathbf{u}_H})^{\sim 1} + \hat{\mathbf{u}}^{\sim 1}\hat{p}^{\sim 1}}_{\text{nonlocal transport}} \right] + F_K^1
\end{aligned}
\tag{3}
$$

where $\mathbf{u} = (u, v, w)$ is the three-dimensional velocity vector, and p is the dynamic pressure. The Γ_K^1 term represents the cross-scale energy transfer to the mesoscale window, which mainly includes the mean kinetic energy (MKE) transfer to EKE ($\Gamma_K^{0\rightarrow1}$), and high-frequency kinetic energy (HKE) transfer to EKE ($\Gamma_K^{2\rightarrow1}$). A key difference between the MS-EVA and other existing energetics formalisms is that the cross-scale energy transfer satisfies a conservation property, i.e, $\sum_{\varpi,n} \Gamma_K^{\varpi} = 0$, where $\varpi = 0, 1, 2$ denote the windows and n denotes the discrete time steps. This important property indicates that Γ_K^{ϖ} is only redistribute energy among scale windows, without creating or consuming energy as a whole. The b^1 term is the conversion between EPE to EKE through baroclinic instability. The nonlocal transport process indicates the EKE is transported into (out of) the domain by energy flux convergence (divergence) through advection and pressure work. Note that the positive (negative) value of terms in the EKE budget indicates that it is the source (sink) of EKE. The F_K^1 term is residual term, indicating the processes which are not explicitly calculated. It includes the external forcing, internal dissipation, and unresolved subgrid processes. As EKE is intensified in the upper 500 m layer in the AR region (figure S1(b), Zhu *et al* 2018, Li *et al* 2023), the EKE budget analysis is performed in the upper 500 m in this study.

The eddy-wind interaction is the mesoscale wind stress work (Renault *et al* 2016, Seo *et al* 2016, Yang *et al* 2019, Jullien *et al* 2020), which can be estimated by

$$W_{\text{Wind}} = \widehat{\mathbf{u}_H}^{\sim1}|_{\text{surface}} \cdot \widehat{\tau}^{\sim1}, \tag{4}$$

where $\mathbf{u}_H^{\sim1}|_{\text{surface}}$ and $\tau^{\sim1}$ are the horizontal surface velocity and surface wind stress in the mesoscale window, respectively. The negative value of W_{Wind} indicates that the eddy-wind interaction serve as eddy killers that remove energy from eddies. We will estimate the contribution of eddy-wind interaction to the F_K^1 term in this study.
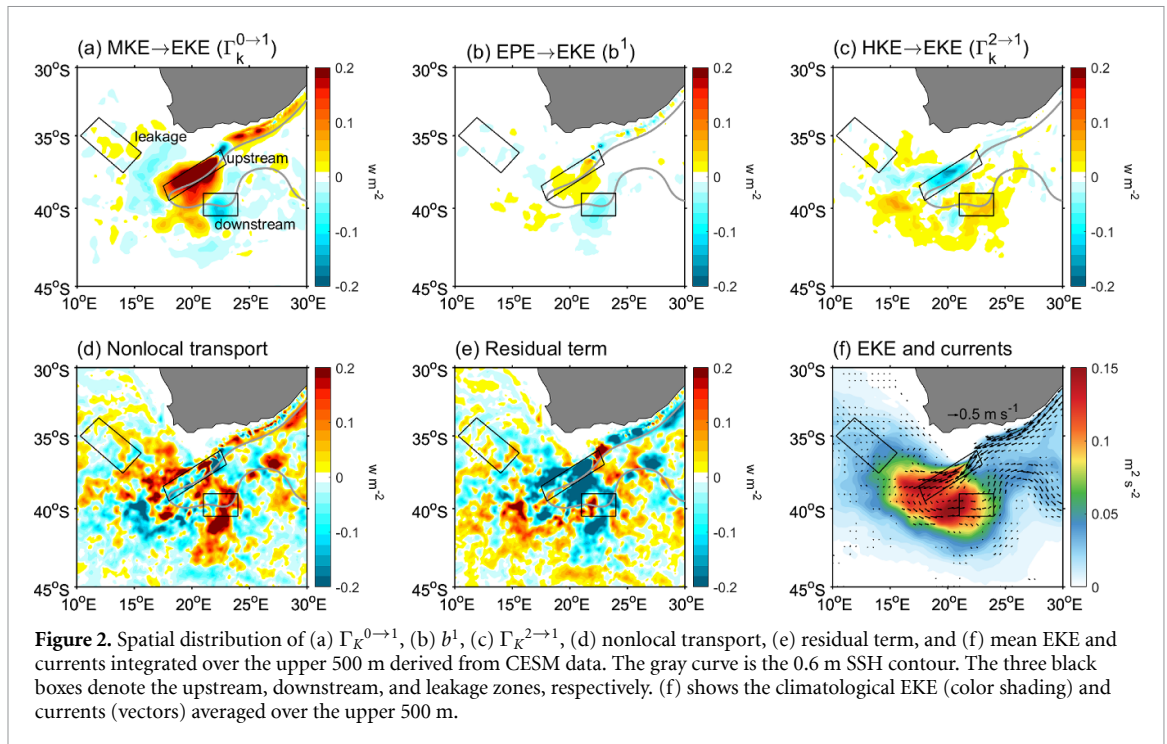
3. Results

3.1. EKE budget in the AR region

Before exploring the dynamics modulating EKE, it is necessary to verify the basin-scale oceanic circulation in the AC system based on model simulations (figure 1). Overall, the mean oceanic circulation and surface velocity estimated from CESM data (figure 1(c)) agree well with those based on altimeter data (figure 1(a)), except for a little difference in the Mozambique Channel, south of Madagascar, and the Antarctic Circumpolar Current regions. The linear spatial correlation between figures 1(a) and (c) is $r = 0.89$. In both data sets, the AC flows southwestward until it reaches the AR point (39° S/15° E), after which the majority of water retroflects, feeding

the eastward ARC. The ARC is characterized by two remarkably stable meander troughs near 26° E and 35° E with a crest in between, which are topographically controlled by the existence of the Agulhas Plateau (Boebel *et al* 2003). In addition to oceanic circulation, The mean surface EKE pattern derived from CESM (figure 1(d)) resembles that from the satellite altimeter (figure 1(b)), with both characterized by the maximum EKE band aligned in the vicinity of AR at 15° E–23° E with a value of about 0.3 m² s⁻². The linear spatial correlation between figures 1(b) and d is $r = 0.87$. Hence, the oceanic circulation and EKE simulated in CESM data aligns markedly well with those derived from the satellite altimeter data in terms of spatial distribution and magnitude. In contrast, the OFES data is largely able to capture the background oceanic circulation in the AC system, but an over-strong mean current penetrate into the Southern Atlantic Ocean at around 10° E (figure 1(e)), where is the Agulhas leakage zone (Biastoch *et al* 2008). The linear spatial correlation between observed surface velocity and OFES velocity is $r = 0.78$. A similar over-strong intrusion to the Southern Atlantic Ocean also exists in the EKE distribution (figure 1(f)), consistent with previous studies suggesting that the Agulhas rings follow a quasi-stable straight pathway in the ocean-alone models (Thoppil *et al* 2011). The correlation between observed surface EKE and OFES EKE is smaller than for CESM, with a value of 0.75. Note that the correlations of observed velocity and EKE with that derived from models do not change much with different time periods selected, and the correlation coefficients between satellite and CESM are higher than that between satellite and OFES (figure S2). Additionally, the EKE level in the AR region is beyond 0.4 m² s⁻² based on the OFES data, significantly larger than that derived from satellite altimeter data. Such systemic biases in EKE distributions, with overestimation and excessive intrusion into the South Atlantic Ocean, commonly occur in ocean-alone models (Maltrud and McClean 2005, Thoppil *et al* 2011, Renault *et al* 2017), indicating that the mesoscale air-sea interaction plays a vital role in modulating EKE in the AR region.

To elucidate the major sources and sinks of EKE in the AR region, the EKE budget integrated over the upper 500 m is diagnosed using CESM data (figure 2). Generally, the dynamic processes modulating EKE are spatially inhomogeneous, particularly in the upstream and downstream zones of the AR (the black boxes in figure 2(a)). Specifically, the $\Gamma_K^{0\rightarrow1}$ (figure 2(a)) exhibits maximum positive value in the upstream zone, indicating that the MKE transfer to EKE through barotropic instability. While the EKE transfer to MKE in the downstream zone with negative $\Gamma_K^{0\rightarrow1}$ spots. Compared to $\Gamma_K^{0\rightarrow1}$, term (figure 2(b)) is one order of magnitude smaller than $\Gamma_K^{0\rightarrow1}$, suggesting that the conversion between EPE and EKE through baroclinic instability is insignificant

Figure 2. Spatial distribution of (a) $\Gamma_K^{0\rightarrow1}$, (b) b^1, (c) $\Gamma_K^{2\rightarrow1}$, (d) nonlocal transport, (e) residual term, and (f) mean EKE and currents integrated over the upper 500 m derived from CESM data. The gray curve is the 0.6 m SSH contour. The three black boxes denote the upstream, downstream, and leakage zones, respectively. (f) shows the climatological EKE (color shading) and currents (vectors) averaged over the upper 500 m.

in generating EKE in the AR region. This is consistent with previous studies (Zhu *et al* 2018, Li *et al* 2023) that have suggested the significant role of barotropic instability in the AR region. Meanwhile, the high-frequency processes obtain energy from mesoscale eddies through forward energy cascade in the upstream zone, while the HKE releases back to EKE through inverse energy cascade in the downstream zone (figure 2(c)). In addition to the cross-scale energy transfer field, the nonlocal transport also exhibits different effects on the upstream and downstream zones of the AR (figure 2(d)). The EKE is generally transported out of the upstream zone by EKE divergence and accumulates in the downstream zone through EKE convergence. This is due to the mean flow carrying low (high) EKE water into the upstream (downstream) and high (low) EKE water out of the domain (figure 2(f)). The residual term F_K^1 (figure 2(e)) reveals overall negative value with minimum in the AR region, suggesting that the F_K^1 is mainly dominated by the dissipation processes associated with the most prominent dissipation in the AR region.

The distributions of processes in the EKE budget equation based on the OFES data (figure S3) are roughly consistent with that derived from CESM data in the upstream and downstream zones, while it exhibits a different pattern in the leakage zone. To find out the dominant mechanism modulating EKE in the three zones, we further quantified every term in the EKE budget equation based on the two datasets (figure 3).

In the upstream zone (figure 3(a)), according to CESM simulations, EKE is mainly generated from MKE through barotropic instability ($\Gamma_K^{0\rightarrow1}$) with

0.25 W m^{-2} and dissipated through dissipation processes with -0.17 W m^{-2}. While in the downstream zone (figure 3(b)), the EKE reservoir dominant fueled by nonlocal transport by 0.06 W m^{-2}. Meanwhile, the destructions of EKE in the downstream zone are mainly through EKE inverse cascade to MKE by -0.04 W m^{-2} and dissipation processes by -0.03 W m^{-2}. The OFES data can roughly capture the dominant source and sink of EKE in the upstream and downstream zones, but the EKE budget in the leakage zone is incorrect. In the leakage zone, the CESM data shows that the EKE is mainly generated through barotropic instability and destructed by nonlocal transport (figure 3(c)). It is largely due to the mean flow does not extend to the leakage zone (figure 2(f)), where the EKE is mainly generated locally through the cross-scale energy transfer field. While in the OFES simulation, the EKE in the leakage zone is generated through nonlocal transport rather than locally. On the one hand, it is due to the eddies propagating westward into the South Atlantic Ocean with weak dissipation in the ocean-alone model (Maltrud and McClean 2005, Thoppil *et al* 2011). On the other hand, the improper over-strong westward intrusion of mean current (figure 1(e)) favors transporting EKE from the upstream zone to the leakage zone (figure S3(f)).

The principal distinction between the OFES and CESM models lies in the absence of mesoscale air-sea interaction in the OFES model, an element integral to the damping of EKE and the shaping of oceanic circulation (Seo *et al* 2016, Jullien *et al* 2020). However, in the AR region, thermal mesoscale air-sea interaction is not imperative for damping EKE, owing to the inconsequential conversion between EPE and EKE
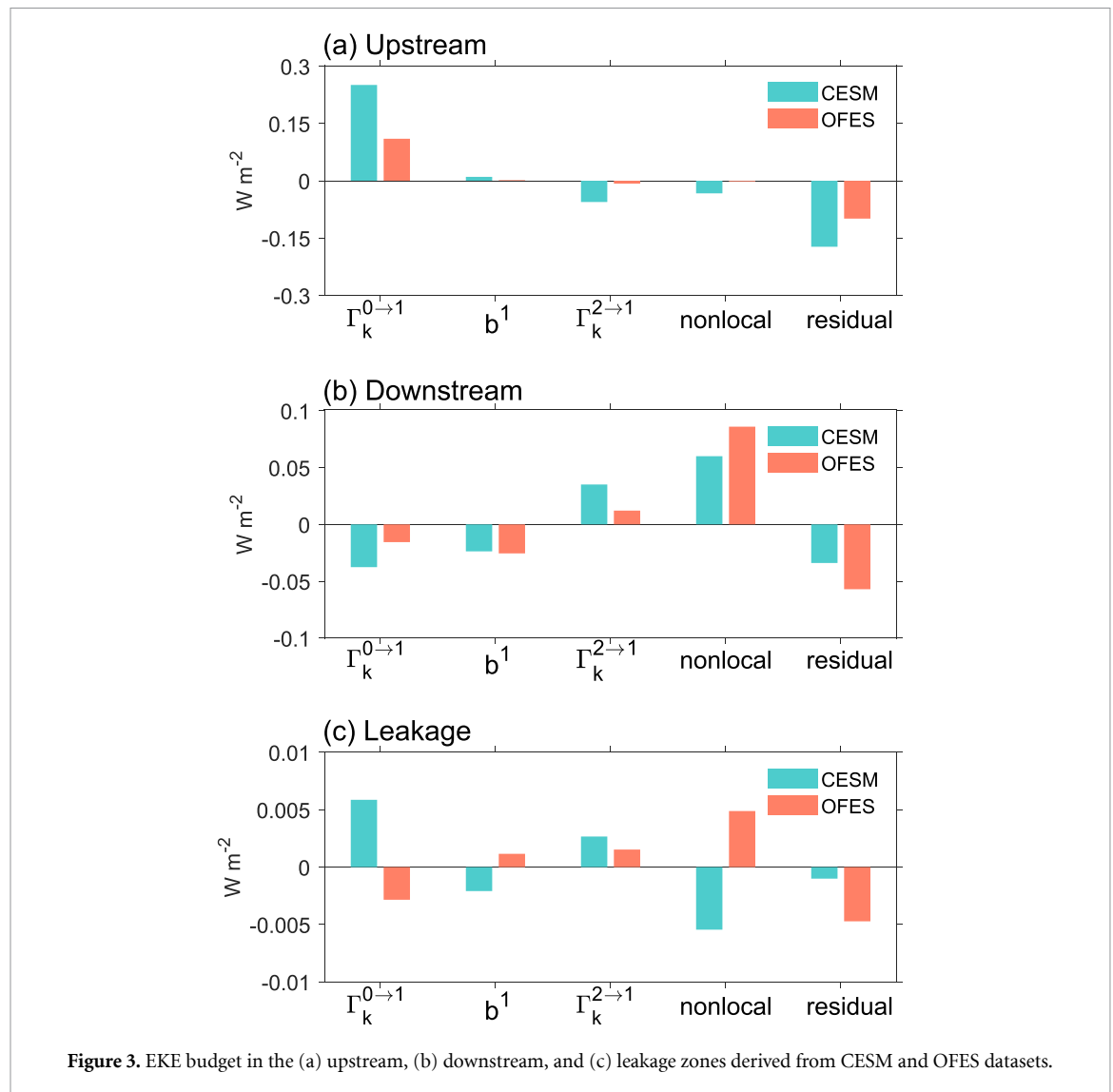
Figure 3. EKE budget in the (a) upstream, (b) downstream, and (c) leakage zones derived from CESM and OFES datasets.

(figure 2(b); Ma *et al* 2016, Renault *et al* 2017). As a result, our investigation will pivot to assessing the role of eddy-wind interaction in moderating EKE in the AR region.

3.2. Potential role of eddy-wind interaction

The eddy-wind interaction acts as the eddy killer that remove energy from mesoscale eddies to the atmosphere (Renault *et al* 2016, Yang *et al* 2019). The CESM-derived W_{Wind} reveals negative centers around the AR regime (figure 4(a)), indicative of pronounced wind stress, responsible for damping mesoscale eddies within the AR region. These zones correlate closely with eddy-shedding positions in the 10° E–23° E range (Zhu *et al* 2021), which are characterized by high EKE levels. Specifically, eddy-wind interaction in the upstream and downstream zones account for ∼12% and ∼36% of the total EKE dissipation, respectively. Compared to the mesoscale wind stress, mesoscale velocities are the primary factors controlling the eddy-wind interaction (figure S4).

While in the OFES simulations, the W_{Wind} (figure 4(b)) is insignificant with a small magnitude in the AR region, indicating that the OFES model cannot accurately represent the eddy-wind interaction in damping EKE. It is worth noting that the W_{Wind} shows positive spots stretching from the upstream zone to the leakage zone in OFES data, suggesting that wind stress is more conducive to eddy generation rather than eddy killer. Therefore, the lack of eddy-wind interaction leads to excessive eddies penetration into the South Atlantic Ocean with weak dissipation in the OFES data.

Meanwhile, the improper over-strong westward intrusion of mean current (figure 1(e)) favors transporting EKE from the upstream zone to the leakage zone (figure S3(f)) in the OFES data. Compared to the CESM model, the wind stress in the OFES model is larger and more westward intrusion (figure S5), which result in an overestimation of total energy input to the ocean by wind work (figure S6; Scott and Xu 2009). It facilitates the mean current in the upstream zone transporting EKE to the leakage zone
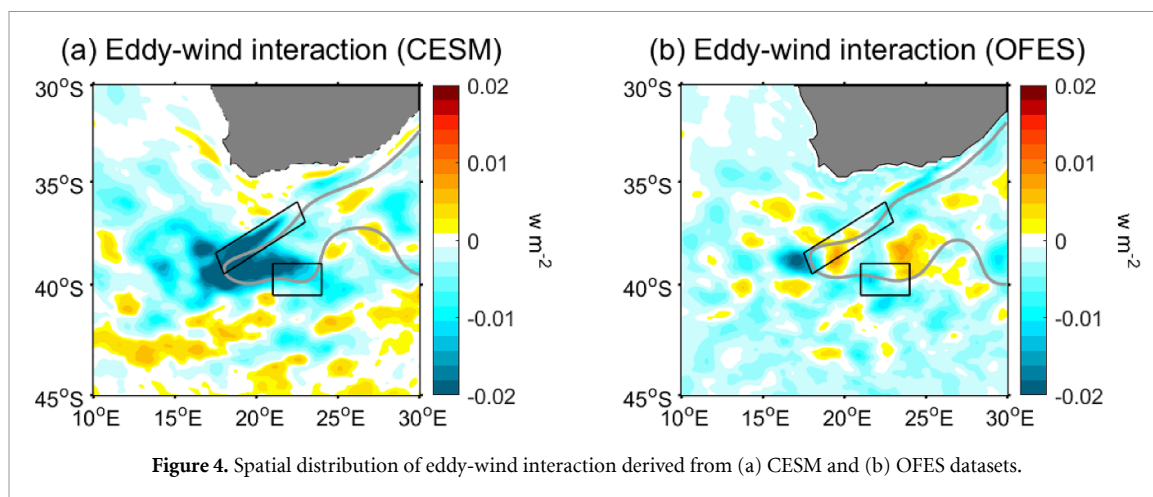
Figure 4. Spatial distribution of eddy-wind interaction derived from (a) CESM and (b) OFES datasets.

in the OFES data. As a result, the EKE in the leakage zone is mainly generated through nonlocal transport rather than locally cross-scale energy transfer in the OFES simulation. Therefore, the above results underline the critical role of eddy-wind interaction in modulating EKE in the AR region, and the lack of eddy-wind interaction in ocean-alone models can results in flawed EKE budget in the leakage zone, leading to severe biases in EKE distribution with overestimation and over-strong penetration into the South Atlantic.

4. Summary

In this study, an EKE budget analysis was performed utilizing CESM simulations, which provide an improved representation of EKE in both distribution and magnitude in the AR region. This study reveals different mechanisms regulating EKE in the upstream, downstream, and leakage zones of the AR. Specifically, in the upstream and leakage zones, the EKE is mainly generated from mean flow through barotropic instability. While in the downstream zone, the EKE reservoir is mainly dominated by nonlocal transport of EKE convergence. Eddy-wind interaction acts as eddy killers that remove energy from mesoscale eddies. Specifically, eddy-wind interaction is pronounced in the AR region, accounting for ∼12% (∼36%) of the total EKE dissipation in the upstream (downstream) zone of the AR in the upper 500 m layer.

However, previous studies reveal that the EKE distribution exhibits common biases (although model-dependent in quantity) in ocean-alone models, typically with overestimation and over-strong penetration of EKE toward the South Atlantic Ocean.

We found that the OFES simulation, with similar resolutions to CESM, can roughly capture the dominant mechanisms responsible for EKE generation in the upstream and downstream zones, while in the leakage zone, the EKE is generated through nonlocal transport of EKE convergence rather than locally cross-scale energy transfer field. The flawed EKE

budget in the leakage zone is due to the lack of eddy-wind interaction in the OFES simulation, leading to insufficient EKE dissipation in the upstream zone and subsequent transport of excessive EKE to the leakage zone. In contrast, in the CESM simulation, the integral eddy-wind interaction dissipates EKE to the atmosphere, resulting in a concentration of EKE within the AR region, and the EKE is generated through locally cross-scale energy transfer in the leakage zone.

Overall, this study suggests the crucial role of eddy-wind interaction in EKE dissipation in the AR region and highlights that mesoscale air-sea interaction, such as eddy-wind interaction, should be taken into consideration in simulations to obtain a realistic representation of both the large-scale and mesoscale circulations in the AR region. It can further improve the estimation of the Agulhas leakage volume transport and contribute to the understanding of the interaction between the Indian and Atlantic Oceans. It is note that in the CESM and OFES models, the AC transport along 32° in the upper 500 m is 50 Sv and 51 Sv, respectively, which are different from the observed mean AC transport of 77 Sv in the upper 3000 m (Beal *et al* 2015). Since the factors affecting the AC strength are complex, the reasons responsible for the underestimation of AC transport in the models needed to be further explored in future studies. In addition, our results present the potential reason responsible for the biases of Agulhas leakage in the ocean-alone models based on the comparison of two models. With the improvement of the eddy-resolving models, we will explore the other reasons in future studies.

Data availability statement

Data used in this study can be downloaded from the websites below:

CESM: https://ibsclimate.org/research/ultra-high-resolution-climate-simulation-project/;

OFES: http://apdrc.soest.hawaii.edu/las_ofes/v6/dataset?catitem=162

ORCID iD

Yanan Zhu ⬤ https://orcid.org/0000-0003-2244-2048

References

Adeagbo O S, Du Y, Wang T and Wang M 2022 Eddy–mean flow interactions in the Agulhas leakage region *J. Oceanogr.* **78** 151–61

Beal L M, De Ruijter W P, Biastoch A and Zahn R 2011 On the role of the Agulhas system in ocean circulation and climate *Nature* **472** 429–36

Beal L M, Elipot S, Houk A and Leber G M 2015 Capturing the transport variability of a western boundary jet: results from the Agulhas current time series experiment (ACT) *J. Phys. Oceanogr.* **45** 1302–24

Biastoch A, Böning C W and Lutjeharms J R E 2008 Agulhas leakage dynamics affects decadal variability in Atlantic overturning circulation *Nature* **456** 489–92

Boebel O, Lutjeharms J, Schmid C, Zenk W, Rossby T and Barron C 2003 The Cape Cauldron: a regime of turbulent inter-ocean exchange *Deep-Sea Res.* II **50** 57–86

Chen H, Schneider E K and Wu Z 2016 Mechanisms of internally generated decadal-to-multidecadal variability of SST in the Atlantic Ocean in a coupled GCM *Clim. Dyn.* **46** 1517–46

Chu J E, Lee S S, Timmermann A, Wengel C, Stuecker M F and Yamaguchi R 2020 Reduced tropical cyclone densities and ocean effects due to anthropogenic greenhouse warming *Sci. Adv.* **6** eabd5109

Dencausse G, Arhan M and Speich S 2010 Spatio-temporal characteristics of the Agulhas current retroflection *Deep-Sea Res.* I **57** 1392–405

Duhaut T H and Straub D N 2006 Wind stress dependence on ocean surface velocity: implications for mechanical energy input to ocean circulation *J. Phys. Oceanogr.* **36** 202–11

Eden C and Dietze H 2009 Effects of mesoscale eddy/wind interactions on biological new production and eddy kinetic energy *J. Geophys. Res.* **114** C5023

Gaube P, Chelton D, Samelson R, Schlax M and O'Neill L 2015 Satellite observations of mesoscale eddy induced Ekman pumping *J. Phys. Oceanogr.* **45** 104–32

Gordon A L 1985 Indian-Atlantic transfer of thermocline water at the Agulhas retroflection *Science* **227** 1030–3

Huang L, Lee S S and Timmermann A 2021 Caspian sea and Black sea response to greenhouse warming in a high resolution global climate model *Geophys. Res. Lett.* **48** e2020GL090270

Hunke E C and Lipscomb W H 2008 The Los Alamos sea ice model user's manual, version 4 *Los Alamos National Laboratory Technical Report* (available at: https://csdms.colorado.edu/w/images/CICE_documentation_and_software_user's_manual.pdf)

Jullien S, Masson S, Oerder V, Samson G, Colas F and Renault L 2020 Impact of ocean–atmosphere current feedback on ocean mesoscale activity: regional variations and sensitivity to model resolution *J. Clim.* **33** 2585–602

Lawrence D M *et al* 2011 Parameterization improvements and functional and structural advances in Version 4 of the community land model *J. Adv. Model. Earth Syst.* **3** M03001

Le Traon P Y, Nadal F and Ducet N 1998 An improved mapping method of multisatellite altimeter data *J. Atmos. Ocean. Technol.* **15** 522–34

Li M, Pang C, Yan X, Zhang L and Liu Z 2023 Energetics of multiscale interactions in the Agulhas retroflection current system *J. Phys. Oceanogr.* **53** 457–76

Liang X S 2016 Canonical transfer and multiscale energetics for primitive and quasigeostrophic atmospheres *J. Atmos. Sci.* **73** 4439–68

Liang X S and Anderson D G 2007 Multiscale window transform *Multiscale Model. Simul.* **6** 437–67

Liang X S and Robinson A R 2005 Localized multiscale energy and vorticity analysis: I. Fundamentals *Dyn. Atmos. Oceans* **38** 195–230

Luo J J, Masson S, Roeckner E, Madec G and Yamagata T 2005 Reducing climatology bias in an ocean–atmosphere CGCM with improved coupling physics *J. Clim.* **18** 2344–60

Lutjeharms J R E and Ansorge I J 2001 The Agulhas return current *J. Mar. Syst.* **30** 115–38

Lutjeharms J R E and Van Ballegooyen R C 1988 The retroflection of the Agulhas current *J. Phys. Oceanogr.* **18** 1570–83

Ma X *et al* 2016 Western boundary currents regulated by interaction between ocean eddies and the atmosphere *Nature* **535** 533–7

Maltrud M E and McClean J L 2005 An eddy resolving global 1/10 ocean simulation *Ocean Modelling* **8** 31–54

Masumoto Y *et al* 2004 A fifty-year eddy-resolving simulation of the world ocean: preliminary outcomes of OFES (OGCM for the earth simulator) *J. Earth Simul.* **1** 35–56

Neale R B *et al* 2012 Description of the NCAR community atmosphere model (CAM 5.0) (No. NCAR/TN-486+STR) (available at: http://doi:10.5065/wgtk-4g06)

Pacanowski R C and Griffies S M 2000 *MOM 3.0 Manual, Technical Report 4* (Geophysical Fluid Dynamics Laboratory) p 680

Pacanowski R 1987 Effect of equatorial currents on surface stress *J. Phys. Oceanogr.* **17** 833–8

Putrasahan D A, Beal L M, Kirtman B P and Cheng Y 2015 A new Eulerian method to estimate "spicy" Agulhas leakage in climate models *Geophys. Res. Lett.* **42** 4532–9

Renault L, McWilliams J C and Penven P 2017 Modulation of the Agulhas current retroflection and leakage by oceanic current interaction with the atmosphere in coupled simulations *J. Phys. Oceanogr.* **47** 2077–100

Renault L, Molemaker M J, McWilliams J C, Shchepetkin A F, Lemarie F, Chelton D, Illig S and Hall A 2016 Modulation of wind work by oceanic current interaction with the atmosphere *J. Phys. Oceanogr.* **46** 1685–704

Sasaki H, Nonaka M, Masumoto Y, Sasai Y, Uehara H and Sakuma H 2008 An eddy resolving hindcast simulation of the quasiglobal ocean from 1950 to 2003 on the Earth simulator *High Resolution Numerical Modeling of the Atmosphere and Ocean* ed K Hamilton and W Ohfuchi (Springer) pp 157–85

Scott R B and Xu Y 2009 An update on the wind power input to the surface geostrophic flow of the World Ocean *Deep-Sea Res.* I **56** 295–304

Seo H, Miller A J and Norris J R 2016 Eddy-wind interaction in the California current system: dynamics and impacts *J. Phys. Oceanogr.* **46** 439–59

Small R J *et al* 2014 A new synoptic scale resolving global climate simulation using the community earth system model *J. Adv. Model. Earth Syst.* **6** 1065–94

Smith R *et al* 2010 The parallel ocean program (POP) reference manual. Ocean component of the community climate

system model (CCSM) p 141 (available at: www.cesm.ucar.edu/models/cesm1.1/pop2/doc/sci/POPRefManual.pdf)

Taburet G, Sanchez-Roman A, Ballarotta M, Pujol M I, Legeais J F, Fournier F and Dibarboure G 2019 DUACS DT2018: 25 years of reprocessed sea level altimetry products *Ocean Sci.* **15** 1207–24

Thoppil P G, Richman J G and Hogan P J 2011 Energetics of a global ocean circulation model compared to observations *Geophys. Res. Lett.* **38** 15

Yang H, Chang P, Qiu B, Zhang Q, Wu L, Chen Z and Wang H 2019 Mesoscale air–sea interaction and its role in eddy energy dissipation in the Kuroshio extension *J. Clim.* **32** 8659–76

Yang Y and San Liang X 2016 The instabilities and multiscale energetics underlying the mean–interannual–eddy interactions in the Kuroshio extension region *J. Phys. Oceanogr.* **46** 1477–94

Yang Y, Weisberg R H, Liu Y and San Liang X 2020 Instabilities and multiscale interactions underlying the loop current eddy shedding in the Gulf of Mexico *J. Phys. Oceanogr.* **50** 1289–317

Zhu Y, Li Y, Zhang Z, Qiu B and Wang F 2021 The observed Agulhas retroflection behaviors during 1993–2018 *J. Geophys. Res.* **126** e2021JC017995

Zhu Y, Qiu B, Lin X and Wang F 2018 Interannual eddy kinetic energy modulations in the Agulhas return current *J. Geophys. Res.* **123** 6449–62